Digest Journal of Nanomaterials and Biostructures Vol. 6, No 4, October - December 2011, p. 1957-1965

# ONE-POT SYNTHESIS OF SILVER-TITANIUM DIOXIDE NANOCOMPOSITES USING ETHYLENE GLYCOL MEDIUM AND THEIR ANTIBACTERIAL PROPERTIES

ALTANGEREL AMARJARGAL[a,b], LEONARD D. TIJING[c], CHEOL SANG KIM[a,c*]

[a]*Department of Bionanosystem Engineering, Graduate School, Chonbuk National University, Jeonju, Jeonbuk 561-756, Korea*

[b]Power Engi*neering School, Mongolian University of Science and Technology, Ulaanbaatar, Mongolia*

[c]*Division of Mechanical Design Engineering, Chonbuk National University, Jeonju, Jeonbuk 561-756, Korea*

We report here for the first time a one-pot simultaneous synthesis and antibacterial properties of Ag-$TiO_2$ nanocomposites via ethylene glycol medium. The salient features of this method include simple operation, large scale production and one medium (solvent) to produce two different nanoparticles. Clusters of Ag and $TiO_2$ nanoparticles with an average size of 20 – 30 nm and narrow size distribution are formed after annealing at 400 and 500 $^oC$. The annealed Ag-$TiO_2$ nanoparticles show excellent antibacterial properties under visible-light irradiation.

(Received September 9, 2011; accepted December 13, 2011)

*Keywords:* Nanocomposite; Synthesis; Composites; Ethylene glycol

## 1. Introduction

Metal oxide nanoparticles with unique properties based on their size, shape, and crystalline structure attract significant attention to various applications [1-3]. Among them, titanium dioxide ($TiO_2$) nanoparticles are one of the popular materials with photocatalytic properties for the disinfection of water [2,4]. Conventional $TiO_2$ photocatalysis needs UV light irradiation due to its high band-gap energy ($E_g$ = 3.2 eV for the anatase corresponding to a wavelength < 390 nm). This requirement leads to considerable energy consumption (fixed UV light source), which restricts its practical application. In recent years, extensive studies have been carried out on the use of visible light for photocatalytic reaction of $TiO_2$ catalysts. In order to extend its working area to the visible light region, $TiO_2$ is usually modified by doping with transition metal ions and with nonmetals, and by dye sensitization. One of the most common strategies of making visible light bio- and photoactive catalysts is by incorporating or depositing metallic silver (Ag) particles onto $TiO_2$ [6-8]. Many methods are used to synthesize Ag-$TiO_2$ nanoparticles, which include sol-gel method followed by hydrothermal reaction [9,10], synthesis of Ag nanoparticles through photoreduction in $TiO_2$ suspension [11], and chemical reduction of $AgNO_3$ precursor and then depositing them on the $TiO_2$ surface [12]. Zhang and Chen [12] reported 98.8% Escherichia coli inhibition using 7.4 wt% Ag/$TiO_2$, which was synthesized by one-pot sol-gel method. Many of the methods for Ag/$TiO_2$ synthesis require complicated processes [9]. In this study, we report a simple, one-pot simultaneous synthesis of Ag-$TiO_2$ nanoparticles using ethylene glycol as medium and poly(vinylpyrrolidone) (PVP) as capping agent. The present method is also called polyol synthesis, which is an excellent method for the synthesis of metal or

*Corresponding author: chskim@jbnu.ac.kr

metal oxide nanoparticles of various shapes [13,14]. To the authors' knowledge, this is the first time that such method is used for the simultaneous synthesis of Ag and $TiO_2$ nanoparticles, i.e. using one medium to produce two different nanoparticles.

## 2. Experimental

### 2.1 Materials

The following chemicals were used as received without further purification: titanium (IV) isopropoxide (TIPP, guaranteed reagent, Junsei), silver nitrate ($AgNO_3$, Showa), poly(vinylpyrrolidone) (PVP, Aldrich, MW-1 300 000), and ethylene glycol ( EG, Showa).

### 2.2 Synthesis of silver-titanium dioxide nanocomposites

In the present study, Ag-$TiO_2$ nanocomposite powder was successfully synthesized by one-step refluxing method using EG medium under ambient conditions. Similar experimental procedure described by Xia and co-workers [14,15] was used in this study with modifications. Ethylene glycol was employed as the reduction medium, silver nitrate ($AgNO_3$) and titanium (IV) isopropoxide as precursors, and PVP as a polymer capping reagent. The schematic layout of the synthesis process is illustrated in Fig. 1. Briefly, 100 ml EG and 1 ml TIPP were refluxed in a three-necked round bottom flask fitted in a heating mantle under vigorous stirring at 170°C for 90 min. Then, 10 mL EG, which was dissolved in 0.33 g PVP that is used to protect the to-be-synthesized silver nanoparticles from agglomeration was added into the hot solution. Soon afterwards, 0.15 M aqueous silver nitrate was introduced into the mixed solution that had already produced titanium glycolate and from this period, the reaction was maintained at 150°C for 30 min. Finally, the solution was cooled to room temperature and the synthesized nanocomposite particles were separated by vacuum filtration. Dark grey precipitate was subsequently washed by de-ionized water and ethanol, and then dried to room temperature for one day. In order to form anatase $TiO_2$, the synthesized nanocomposites were annealed at different temperatures: 400 and 500°C.

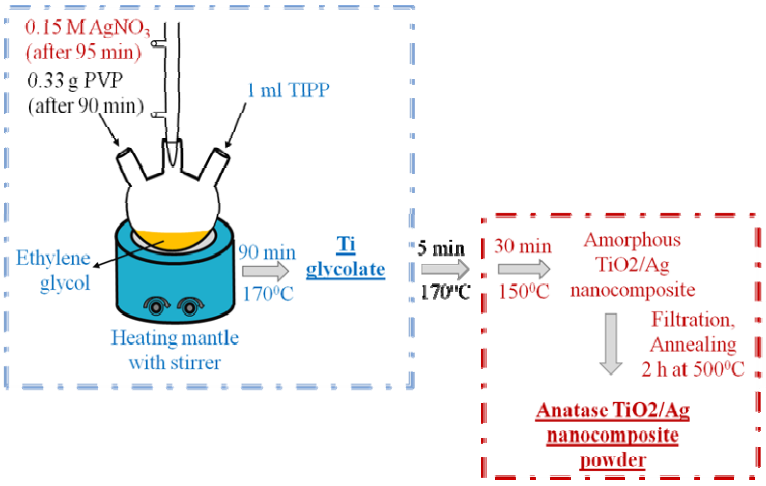


*Fig. 1. Schematic layout and procedure of the Ag/$TiO_2$ synthesis in the present study.*

### 2.3 Characterization

The surface structure and morphology of the present Ag-$TiO_2$ nanocomposite powder were studied by field emission scanning electron microscopy (FE-SEM, S-7400, Hitachi, Japan),

and the elemental composition was checked using an energy dispersive spectrometer (EDS). The particle size and distribution were determined using a transmission electron microscope (TEM, JEOL JEM, Japan) at an accelerating voltage of 200 kV. X-ray powder diffraction (XRD) analysis was carried out by a Rigaku X-ray diffractometer (Cu Kα, λ = 1.54059 Å) over Bragg angles ranging from 20 to 80°. Surface state of samples was surveyed by X-ray photoelectron spectroscopy (XPS, AXIS-NOVA, Kratos, Inc.) with an Al Kα irradiation source.

### 2.4 Bacterial inactivation test

For bacterial inactivation test, E. coli Top 10 strain was used as the model microorganism. Escherichia coli was grown in lysogeny broth (LB) containing tryptone, yeast extract, sodium chloride and distilled water in right proportions. Before inoculating bacteria, LB was first sterilized by autoclaving for 20 min at 121°C and 15 psi. One colony of E. coli was taken out from the original stock in an agar plate and was cultured in LB medium at 2 ml. This bacterial solution was incubated at 35 ±0.1°C and 200 rpm for 24 hr using a shaking incubator. The working suspensions were prepared by adding 2 ml of inoculated LB medium to a 400 ml sterilized distilled water in a beaker. The antibacterial experiments were carried out in a sterilized 100 ml glass beaker containing E. coli suspension (60 ml) and 0.08 g/L of Ag-$TiO_2$ photocatalysts, mixed by magnetic stirring. The initial bacterial concentration was maintained at $10^7$ CFU/ml and the tests were performed at room temperature for a duration of 120 min. A 32-W fluorescent lamp was used as visible light source to trigger the photocatalytic reaction. The baseline test was performed using a bacterial suspension without photocatalyst irradiated with visible light, and a reaction mixture with no visible light irradiation was used as a dark control. At given time intervals, 1 ml suspension was collected and diluted appropriately by serial dilution in distilled water. Sampling was done in triplicates and the average was calculated together with the standard deviation. To count the bacterial concentration, ready-to-use petrifilm (3M Petrifilm, USA) and prepared agar plates were used to plate the samples. After incubation for 48 hrs, the number of bacteria was manually counted using a colony counter.

## 3. Results and discussion

The separate synthesis of Ag and $TiO_2$ in the form of nanowires and nanorods with high aspect ratio has already been successfully fabricated by many researchers [16, 17]. Here, we present a simple and simultaneous one-pot synthesis of Ag-$TiO_2$ nanoparticles using ethylene glycol as medium. Figures 2 and 3 show the FE-SEM and TEM images, respectively of the as-synthesized and annealed Ag-$TiO_2$ nanocomposite powders. The as-synthesized samples (Fig. 2a) obtained were in the shape of nanorods (diameter ~ 50 nm; length ~ several hundred nanometers). The darkened clusters in Fig. 3a are the Ag nanorods as confirmed by EDS (Fig. 3d), while the grey areas are the amorphous titanium glycolate. Strong Ag peaks could be observed in the as-synthesized samples. On the other hand, the heat-treated samples (Figs. 2b, and Figs. 3a-c) showed clusters of smaller nanoparticles with an average size of 20 – 30 nm with a narrow size distribution. The EDS results for heat-treated samples at 400 and 500°C (Figs. 3e and 3f, respectively) showed dominant high peaks of Ag, signifying that the dark particles are silver [12]. Under high annealing conditions, the titanium glycolate were transformed into anatase $TiO_2$, and these $TiO_2$ nanoparticle clusters were dispersed over the bigger Ag nanoparticle clusters. In the present synthesis, titanium glycolate was first produced from the heating of titanium alkoxide in ethylene glycol medium [16], and then the hot ethylene glycol solution reduced the silver nitrate, followed by the nucleation of metallic silver and growth of silver nanoparticles [18]. The simultaneous synthesis of Ag-$TiO_2$ nanocomposites could be attributed to the process known as Ostwald ripening [15]. Du et al. [19] obtained similar morphology of Ag-$TiO_2$ core shell nanowires using a different method. They suggested a template-induced Oswald ripening mechanism to explain the formation of the Ag/$TiO_2$ core-shell nanowires.

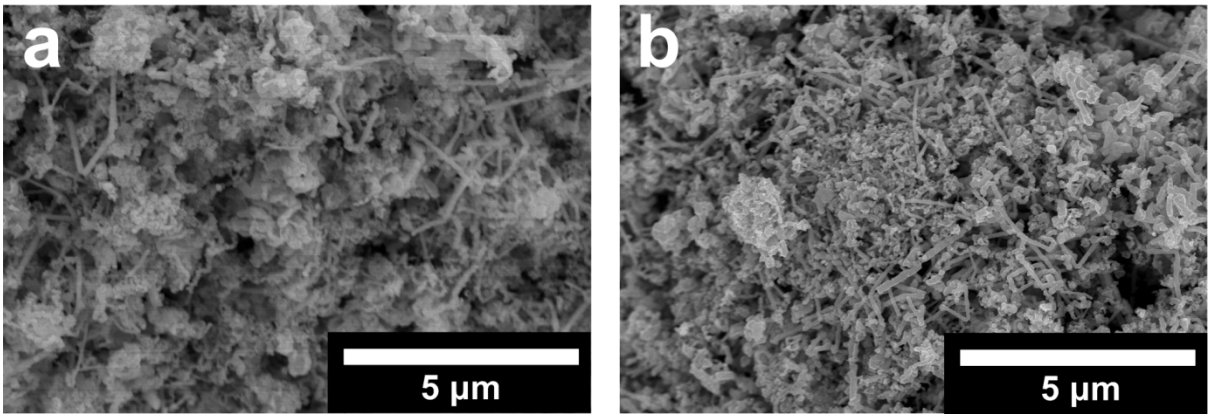


*Fig. 2. SEM images of (a) as-synthesized and (b) annealed at 500°C Ag-$TiO_2$ nanocomposite powders.*

We used high molecular weight PVP as capping agent to help lessen the particle aggregation, but still the nanoparticles obtained were in aggregates of Ag nanoparticles, which coalesce with primary nanoparticles. This aggregation phenomenon was also observed by Cho et al. [20]. Liu et al. [21] also used high molecular weight PVP and reported a successful synthesis of silver nanostructures with controlled morphology and crystal structure. They reported that the control on the shape is attributed to the different capping modes for the PVP-directed Ag nanocrystal growth. They further demonstrated that the product of the polyol process using high molecular weight PVP polymer as capping agent can be Ag nanoparticles, straight nanorods or zigzag nanorods, depending on the reaction parameters. In the present study, because of the relatively high temperature used in the synthesis of silver particles, the Brownian motion and mobility of surface atoms increased, which enhanced the probability of particle collision, adhesion, and subsequent coalescence [18]. Shin et al. [22] deduced the following three-step mechanism for the growth of silver nanoparticles: (i) silver ions interact with PVP; (ii) nearby silver atoms that have been reduced by $\gamma$ -irradiation aggregate at close range (the primary nanoparticles); and (iii) nearby primary nanoparticles coalesce with other primary nanoparticles or interact with PVP molecules to form larger aggregates (secondary nanoparticles).

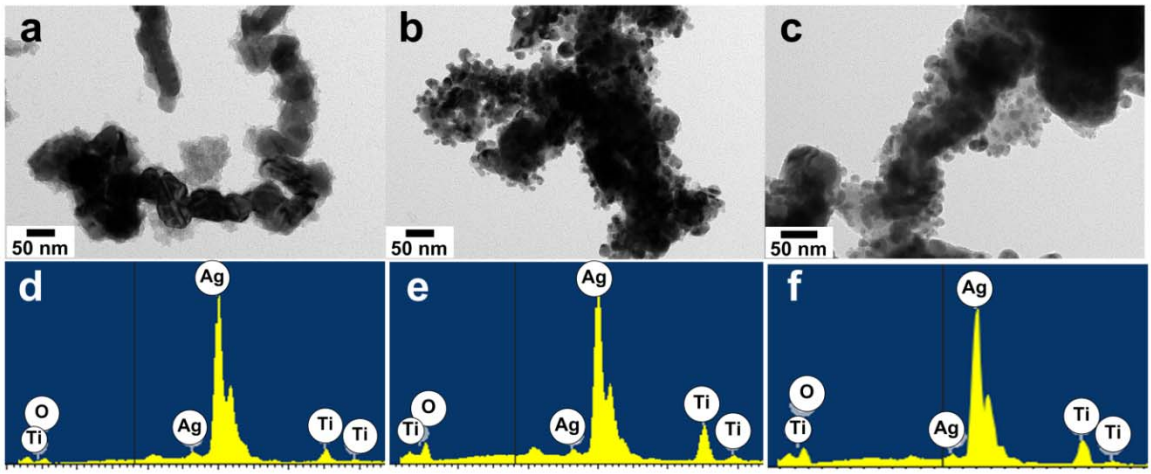


*Fig. 3. TEM images (a-c) and EDS profiles (d-f) of as-synthesized (a, d), and annealed at 400°C (b, e) and 500°C (c, f) Ag-$TiO_2$ nanocomposite powders.*

Figure 4 shows the XRD spectra of as-synthesized and annealed Ag-$TiO_2$ nanocomposite particles at different temperatures. The obtained XRD spectra of the annealed Ag-$TiO_2$ nanocomposite sample at 500°C compounded the silver nanoparticles, which possessed good

crystallinity and high purity with 2θ values of 37.9, 44.1, 64.2, and 77.1°, corresponding to the (111), (200), (220) and (311) planes, respectively, and two peaks, at 2θ values of 24.9 and 48.4°, corresponding to the (101) and (200) planes of anatase $TiO_2$ nanoparticles, respectively [10]. The XRD spectra of annealed Ag-$TiO_2$ powders at 400°C did not indicate anatase $TiO_2$ peaks due to the detection limit of apparatus or a possible high content of silver nitrate precursor, but growth of crystallites could still be observed in the TEM image (Fig. 3b). In the case of as-synthesized nanocomposite, because the powders contained amorphous titanium glycolate, the spectra for anatase crystalline form could not be detected [19,23,24].

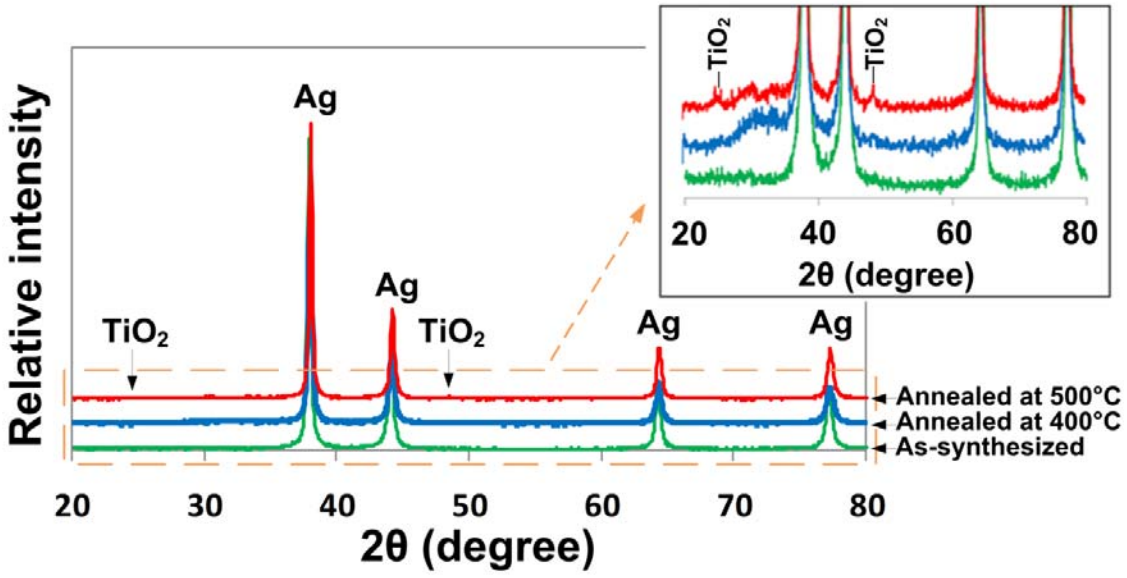


*Fig. 4. XRD spectra of the synthesized and annealed Ag/$TiO_2$ nanoparticles (inset shows magnified peaks of $TiO_2$).*

More information on the elemental composition and oxidation states of elements in the Ag-$TiO_2$ nanocomposite powder are provided by XPS. XPS spectra indicated that all three samples contained Ag, Ti, O and C elements (Fig. 5). Weak and unexpected peak for C1s (282.2 eV) has been associated with not only the residual carbon from the sample, but also adventitious hydrocarbon from the XPS instrument itself. The annealed samples have a much lower carbon content compared to the as-synthesized sample due to their thermal decomposition. Figures 5b-d show high-resolution XPS spectra of Ag 3d (Fig. 5b), Ti 2p (Fig. 5c) and O 1s (Fig. 5d) core levels in the Ag-$TiO_2$ nanocomposites. In both annealed samples, the peaks observed at 368.3 and 374.3 eV can be ascribed to Ag $3d_{3/2}$ and Ag $3d_{5/2}$ of the metallic silver and no peak corresponding to $Ag_2O$ or AgO was detected. These results are in good agreement with the XRD characterization. Furthermore, the binding energy values of Ti $2p_{3/2}$ and O 1s peaks show that they are in the range 458.15 – 458.4 eV and 529.85 eV, respectively. These values can be attributed to $Ti^{4+}$ and $O^{2}$ in $TiO_2$ [6,9,19]. For the as-synthesized Ag/$TiO_2$, the Ti 2p and Ag 3d peaks shifted down to lower binding energy, indicating that the chemical environment of Ti and Ag atoms was changed [21,25].

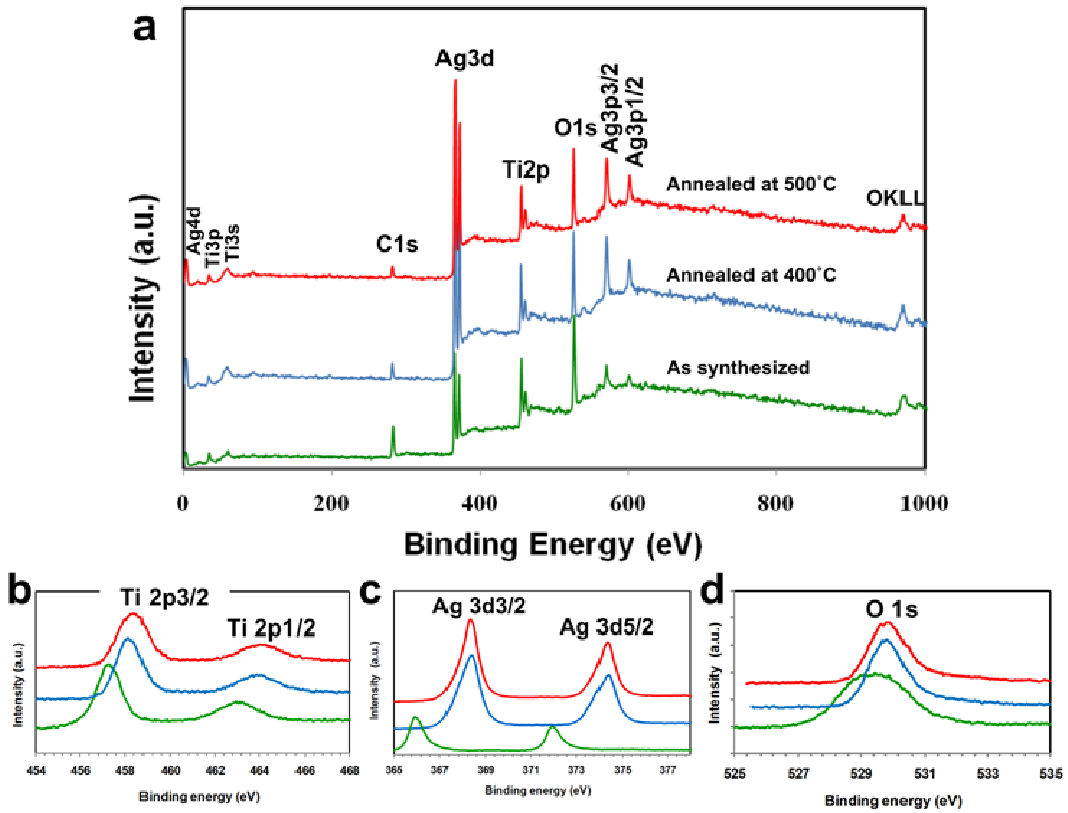


*Fig. 5. XPS spectra of the synthesized Ag/$TiO_2$ nanoparticles; (b) – (d) show high-resolution XPS spectra of Ag 3d, Ti 2p, and O 1s, respectively.*

The photocatalytic properties of the Ag-$TiO_2$ nanocomposite powder was evaluated by inactivation of E. coli bacteria under visible light irradiation for 120 min. Figure 6 shows the antibacterial test results at an initial concentration of $10^7$ CFU/ml. The baseline test showed an almost constant concentration of E. coli after 120 min, signifying that, only visible light could not inactivate E. coli for this duration. When as-synthesized Ag-$TiO_2$ nanoparticles were used, a 2-log decrease was observed after 120 min of test. This low efficiency could be attributed to the amorphous structure of the $TiO_2$ nanoparticles, and to the changes of environment affecting Ag nanoparticles, as confirmed by XPS. The annealed Ag-$TiO_2$ nanoparticles showed excellent antibacterial properties under visible-light irradiation. Ag-$TiO_2$ nanoparticles annealed at 400$^o$C showed a 100% bacterial inactivation after 90 min, while the Ag-$TiO_2$ nanoparticles annealed at 500$^o$C revealed better antibacterial efficiency, killing all bacteria only after 60 min. The differences in result could be attributed to the differences in crystallinity and sizes of the nanoparticles. We also checked whether the synthesized nanoparticles could inactivate bacteria without visible-light irradiation (i.e., dark control). The annealed Ag-$TiO_2$ at 500$^o$C in dark still showed good antibacterial properties showing an 8-log decrease after 120 min of test. This is primarily due to the antimicrobial activity of Ag itself [26] with good crystallinity and high purity. Optical images of bacterial concentration as checked by plating in agar dishes in Fig. 7 clearly show the reduction in bacterial colony through time.

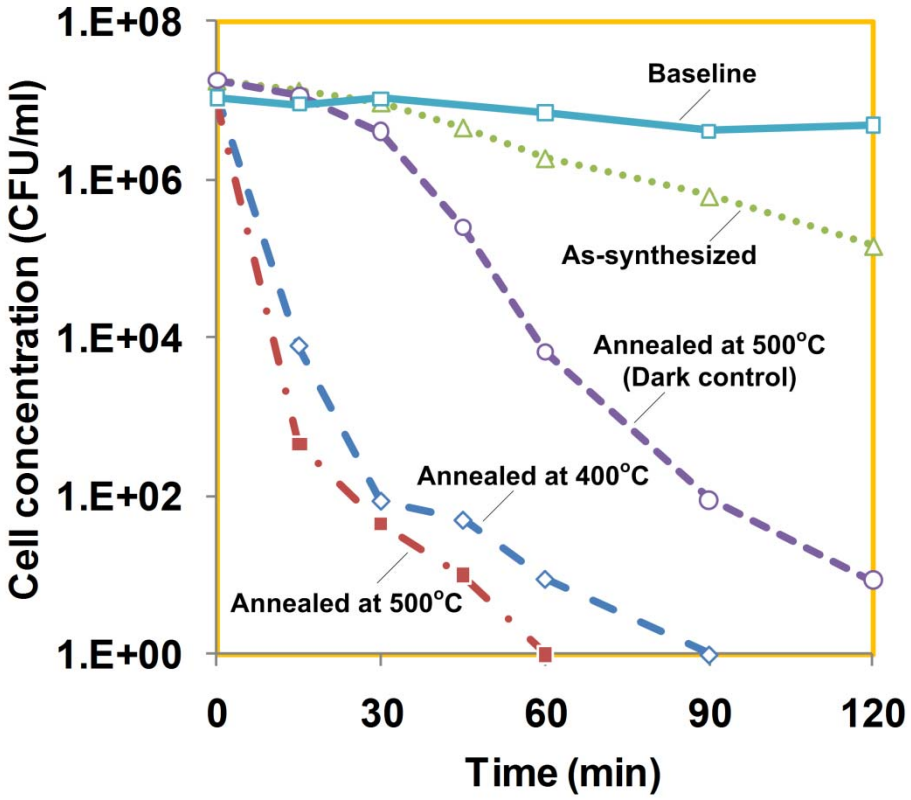


*Fig. 6. Bacteria concentration versus time for all samples under visible light and in the dark.*

The photocatalytic activity of $TiO_2$ depends on its crystal phase, crystallite size and crystallinity. It is known that the anatase form of $TiO_2$ crystallite with small crystallite size and high crystallinity exhibits better photocatalytic property [27]. On the other hand, the bactericidal effect of Ag nanoparticles is still not fully understood but some of the killing mechanisms involved are the following: (a) Ag nanoparticles adhere and attach on cell membrane causing structural changes and damage [12]; (b) Ag nanoparticles can get inside the bacterial membrane, which damages DNA and replication ability [8,12], and; (c) release of Ag ions from the dissolution of silver and formation of free radicals on Ag particles which inhibit bacteria [8]. Silver accepts electrons at an energy just below the conduction band, and it helps in trapping the electron from the conduction band after light absorption and charge separation, which limits the threat of recombination after the hole oxidizes water and form hydroxyl radicals [8]. The synergistic effect of both $TiO_2$ and Ag with visible-light irradiation gives excellent antibacterial properties of the synthesized nanoparticles.

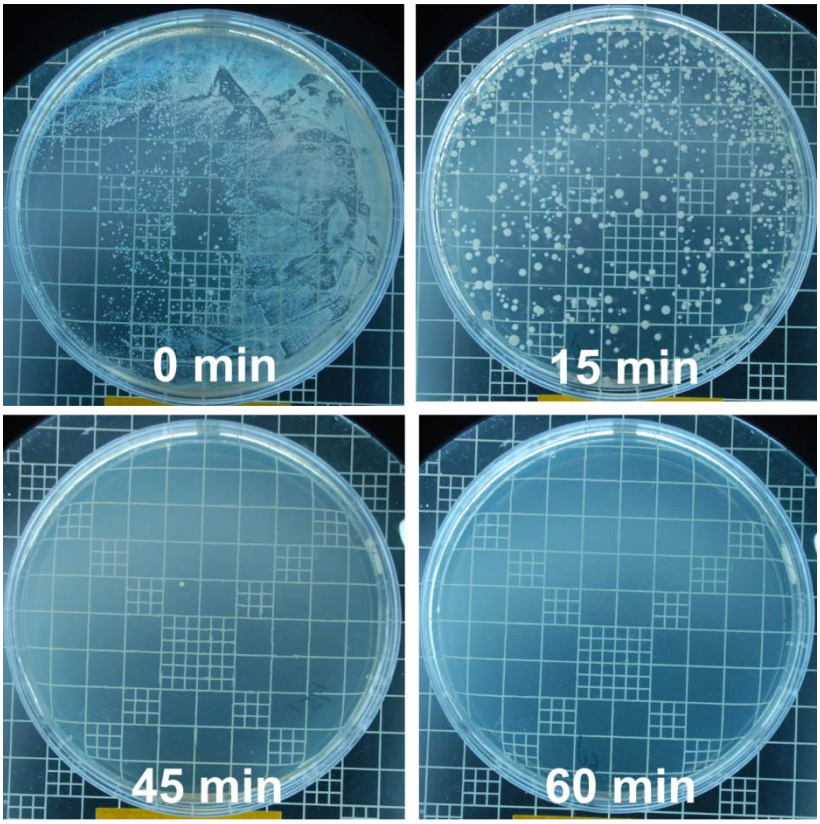


*Fig. 7. Optical photographs of the antibacterial activity results of the Ag-$TiO_2$ sample annealed at 500°C and irradiated with visible light for 120 min.*

## 4. Summary

In summary, we report here a simple refluxing method to synthesize Ag-$TiO_2$ nanocomposite using one medium. Samples were characterized by field emission scanning electron microscopy (FE-SEM), transmission electron microscopy (TEM), X-ray diffraction (XRD) and X-ray photoelectron spectroscopy (XPS). Furthermore, their antibacterial properties were evaluated using E. coli as model organism under visible light irradiation. The obtained Ag-$TiO_2$ nanocomposites indicated that they have good crystallinity, high purity and excellent antibacterial properties.

### Acknowledgements

This research was supported by a grant from the Korean Ministry of Education, Science and Technology through the Regional Core Research Program/ Center for Healthcare Technology Development (Project no. 1345110369) and partially by a grant from the Business for International Cooperative Research and Development between Industry, Academy and Research Institute funded by the Korean Small and Medium Business Administration (Project no. 00042172-1).

## References

[1] H.J. Kim, K.J. Shin, M.K. Han, K.J. An, J.K. Lee, I. Honma, H.S. Kim, Scripta Mater., **61**, 1137 (2009).
[2] D.I. Hadaruga, N.G. Hadaruga, C. Lazau, C. Ratiu, C. Craciun, I. Grozescu, Dig. J. Nanomater. Bios., **5** (4), 919 (2010).

[3] S. Vlad, C. Ciobanu, R.V. Gradinaru, L.M. Gradinaru, A. Nistor, Dig. J. Nanomater. Bios., **6**(3), 921 (2011).
[7] R. van Grieken, J. Marugan, C. Sordo, C. Pablos, Catal Today, **144**, 48 (2009).
[8] L. Cui, F. huang, M. Niu, L. Zeng, J. Xu, Y. Wang, J. Mol. Catal. A, **326**, 1 (2010).
[9] L. Mai, D. Wang, S. Zheng, Y. Xie, C. Huang, Z. Zhang, Appl. Surf. Sci., **257**, 974 (2010).
[10] K.D. Kim, D.N. Han, J.B. Lee, H.T. Kim, Scripta Mater., **54**, 143 (2006).
[11] A.A. Ashkarran, S.M. Aghigh, M. Kavianipour, N.J. Farahani, Curr. Appl. Phys., **11**, 1048 (2011).
[12] Y. Lai, Y. Chen, H. Zhuang, C. Lin, Mater. Lett., **62**, 3688 (2008).
[13] B. Cheng, Y. Le, J. Yu, J. Hazard. Mater., **177**, 971 (2010).
[14] S.F. Chen, J.P. Li, K. Qian, W.P. Xu, Y. Lu, W.X. Huang, S.H. Yu, Nano Res., **3**, 244 (2010).
[15] H. Zhang, G. Chen, Environ. Sci. Technol., **43**, 2905 (2009).
[16] F. Fievet, J.P. Lagier, B. Blin, B. Beaudoin, M. Figlarz, Solid State Ionics, **32** (3), 198 (1989).
[17] X. Jiang, Y. Wang, T. Herricks, Y. Xia, J. Mater. Chem., **14**, 695 (2004).
[18] Y. Sun, B. Gates, B.T. Mayers, Y. Xia, Nano Lett., **2**, 165 (2002).
[19] S. Priya, J. Robichaud, M-C. Me´thot, S. Balaji, J. Ehrman, B.L. Su, Y. Djaoued, J. Mater. Sci., **44**, 6470 (2009).
[20] R. Becker, F. Söderlind, B. Liedberg, P. Käll, Mater. Lett., **64**, 956 (2010).
[21] D. Kim, S. Jeong, J. Moon, Nanotechnology, **17**, 4019 (2006).
[22] J. Du, J. Zhang, Z. Liu, B. Han, T. Jiang, Y. Huang, Langmuir, **22**, 1307 (2006).
[23] M.S. Cho, S.G. Kim, I. Kim, B.W. Kim, Y.K. Lee, Macromol. Res. **18**, 1070 (2010).
[24] X. Liu, F. Zhang, R. Huang, C. Pan, and J. Zhu, Cryst. Growth Des., **8**, 1916 (2008).
[25] H. S. Shin, H. J. Yang, S. B. Kim, M. S. Lee, J. Colloid Interface Sci., **274**, 89 (2004).
[26] D. Wang, R. Yu, N. Kumada, N. Kinomura, Chem. Mater., **11**, 2008 (1999).
[27] A. Zielinska, E. Kowalska, J.W. Sobczak, I. Łacka, M. Gazda, B. Ohtani, J. Hupka, A. Zaleska, Sep. Purif. Technol., **72**, 309 (2010).
[28] Y.L. Kuo, H.W. Chen, Y. Ku, Thin Solid Films, **515**, 3461 (2007).
[29] A. Dror-Ehre, H. Mamane, T. Belenkova, G. Markovich, A. Adin, J. Colloid Interf. Sci., **339**, 521 (2009).
[30] L. Gao, Q. Zhang, Scripta Mater. **44**, 1195 (2001).